REPORT DOCUMENTATION PAGE

Form Approved
OMB No. 0704-0188

PLEASE DO NOT RETURN YOUR FORM TO THE ABOVE ORGANIZATION.

1. REPORT DATE *(DD-MM-YYYY)*	2. REPORT TYPE	3. DATES COVERED *(From - To)*
20-12-2011	Journal Article	

4. TITLE AND SUBTITLE
Light-absorbing Components in Lake Superior

5a. CONTRACT NUMBER

5b. GRANT NUMBER

5c. PROGRAM ELEMENT NUMBER
N/A

6. AUTHOR(S)
Steven Effler, MaryGail Perkins, Feng Peng, Christopher Strait, Alan Weidemann, Martin Auer

5d. PROJECT NUMBER
NNH09AM26I

5e. TASK NUMBER

5f. WORK UNIT NUMBER
73-4223-09-5

7. PERFORMING ORGANIZATION NAME(S) AND ADDRESS(ES)
Naval Research Laboratory
Oceanography Division
Stennis Space Center, MS 39529-5004

8. PERFORMING ORGANIZATION REPORT NUMBER
NRL/JA/7330-10-0443

9. SPONSORING/MONITORING AGENCY NAME(S) AND ADDRESS(ES)
NASA Headquarters
Attn: Laurie Friederich
Mail Code 210.H, Bldg. 17, Rm. N111
Greenbelt, MD

10. SPONSOR/MONITOR'S ACRONYM(S)
NASA

11. SPONSOR/MONITOR'S REPORT NUMBER(S)

12. DISTRIBUTION/AVAILABILITY STATEMENT
Approved for public release, distribution is unlimited.

13. SUPPLEMENTARY NOTES
20120113181

14. ABSTRACT
Features of light absorption are critical to optical aspects of water quality and in regulating the signal available for remote sensing. Spectral characteristics and spatial patterns of light-absorbing components, and their relationships with optically active constituents, are documented for the Sturgeon River, Keweenaw Bay, and Lake Superior based on analyses of samples collected on two cruises (2006 and 2007, 20 sites). The absorption coefficient, a (m− 1), is partitioned according to the additive components (ax) of colored dissolved organic matter (aCDOM), non-algal particles (aNAP), phytoplankton (aϕ), and water itself (aw; known). The role of minerogenic particles and their iron content in regulating aNAP is evaluated based on paired measurements by an individual particle analysis technique (Peng et al., 2009), through empirical analyses and Mie theory calculations of absorption by these particles (am). Spectral characteristics of aNAP and aϕ were consistent with those reported for other case 2 (i.e., phytoplankton not dominant) systems. However, the slope values that describe aCDOM spectra for the bay and the lake were unusually low, suggesting an atypical composition for the lake's CDOM. The dominant absorbing component in the blue wavelengths was CDOM, representing ≥ 75% of a at a wavelength of 440 nm at all sites in the 2006 survey. A general gradient in both aCDOM and aNAP extended from the Sturgeon River, through the bay, into eastern Lake Superior in that survey. Relationships between ax and optically active constituents were within the broad ranges reported for other case 2 systems. Minerogenic particles, related to their iron content, are demonstrated to be an important component of aNAP.

15. SUBJECT TERMS
light absorption, remote sensing, minerogenic particles, Lake Superior

16. SECURITY CLASSIFICATION OF:			17. LIMITATION OF ABSTRACT	18. NUMBER OF PAGES	19a. NAME OF RESPONSIBLE PERSON
a. REPORT	b. ABSTRACT	c. THIS PAGE			Alan Weidemann
Unclassified	Unclassified	Unclassified	UL	10	19b. TELEPHONE NUMBER *(Include area code)* (228) 688-6232

Journal of Great Lakes Research 36 (2010) 656–665

Contents lists available at ScienceDirect

Journal of Great Lakes Research

journal homepage: www.elsevier.com/locate/jglr

Light-absorbing components in Lake Superior

Steven W. Effler [a,*], MaryGail Perkins [a], Feng Peng [a], Christopher Strait [a], Alan D. Weidemann [b], Martin T. Auer [c]

[a] Upstate Freshwater Institute, P.O. Box 506, Syracuse, NY, 13214, USA
[b] Naval Research Laboratory, Stennis Space Center, MS, 39529, USA
[c] Department of Civil and Environmental Engineering, Michigan Technological University, 1400 Townsend Drive, Houghton, MI, 49931, USA

ARTICLE INFO

Article history:
Received 13 January 2010
Accepted 14 July 2010

Communicated by Joseph De Pinto

Index words:
Lake Superior
Light absorption
Minerogenic particles
Remote sensing

ABSTRACT

Features of light absorption are critical to optical aspects of water quality and in regulating the signal available for remote sensing. Spectral characteristics and spatial patterns of light-absorbing components, and their relationships with optically active constituents, are documented for the Sturgeon River, Keweenaw Bay, and Lake Superior based on analyses of samples collected on two cruises (2006 and 2007, 20 sites). The absorption coefficient, a (m^{-1}), is partitioned according to the additive components (a_x) of colored dissolved organic matter (a_{CDOM}), non-algal particles (a_{NAP}), phytoplankton (a_ϕ), and water itself (a_w; known). The role of minerogenic particles and their iron content in regulating a_{NAP} is evaluated based on paired measurements by an individual particle analysis technique (Peng et al., 2009), through empirical analyses and Mie theory calculations of absorption by these particles (a_m). Spectral characteristics of a_{NAP} and a_ϕ were consistent with those reported for other case 2 (i.e., phytoplankton not dominant) systems. However, the slope values that describe a_{CDOM} spectra for the bay and the lake were unusually low, suggesting an atypical composition for the lake's CDOM. The dominant absorbing component in the blue wavelengths was CDOM, representing ≥75% of a at a wavelength of 440 nm at all sites in the 2006 survey. A general gradient in both a_{CDOM} and a_{NAP} extended from the Sturgeon River, through the bay, into eastern Lake Superior in that survey. Relationships between a_x and optically active constituents were within the broad ranges reported for other case 2 systems. Minerogenic particles, related to their iron content, are demonstrated to be an important component of a_{NAP}.

Introduction

The magnitude of the light absorption coefficient (a; unit of 1/length, m^{-1}), an inherent optical property (IOP; i.e., independent of the geometry of the light field), is the fraction of the radiant flux absorbed divided by the thickness of the layer (Kirk, 1994). The magnitude of a varies as a function of wavelength (λ), according to the composition of water with respect to light absorbing constituents (Kirk, 1994; Babin et al., 2003b). The magnitude and spectral character of a are determinants of apparent optical properties (AOPs; those that depend on the geometry of the light field), such as the diffuse attenuation coefficient and remote sensing reflectance.

Usually, $a(\lambda)$ is partitioned into four additive components (a_x; Babin et al., 2003b)

$$a(\lambda) = a_W(\lambda) + a_\phi(\lambda) + a_{NAP}(\lambda) + a_{CDOM}(\lambda) \quad (1)$$

that include contributions from pure water (w), phytoplankton (ϕ), non-algal particles (NAP), and colored dissolved organic matter (CDOM, or gelbstoff). Absorption by pure water increases in red wavelengths, and is well defined (Pope and Fry, 1997). Phytoplankton demonstrate a broad absorption peak at ~440 nm and a more well defined maximum at 676 nm (Kirk, 1994; Babin et al., 2003b). Both a_{NAP} and a_{CDOM} decrease exponentially with increasing λ over the visible wavelengths (Babin et al., 2003b; Perkins et al., 2010). Knowledge of a, its components (a_x), and their spectral characteristics is important for developing and validating remote sensing algorithms for water quality and mechanistic optics models for the underwater light field (Effler et al., 2008), and advancing related initiatives for the Laurentian Great Lakes (Gons and Auer, 2004; Gons et al., 2008). Establishment of relationships between a_x and concentrations of optically active constituents, such as total suspended solids (TSS) and chlorophyll a (Chl), is necessary to support mechanistic approaches to estimate their patterns through remote sensing.

Case 1 waters (open oceans) are those where patterns in optical properties are driven by distributions of phytoplankton, and NAP and CDOM covary with, and are subordinate to, the phytoplankton component (Morel and Prieur, 1977). In contrast, in case 2 waters, such as coastal marine and lacustrine systems, NAP and CDOM do not necessarily covary with phytoplankton and may not be subordinate. Direct quantification of a_x in lacustrine systems remains rare (Binding et al., 2008; Perkins et al., 2009, 2010), despite the establishment of standardized laboratory protocols for a_ϕ, a_{NAP} and a_{CDOM} for marine

* Corresponding author.
E-mail address: sweffler@upstatefreshwater.org (S.W. Effler).

0380-1330/$ – see front matter © 2010 International Association for Great Lakes Research. Published by Elsevier B.V. All rights reserved.
doi:10.1016/j.jglr.2010.08.001

initiatives (Mitchell et al., 2003). Resolution and quantification of NAP have received the least attention of the components (Babin et al., 2003b). Moreover, there exists great uncertainty concerning NAP's composition, particularly related to contributions of minerogenic versus organic (e.g., detritus) particles (Bowers et al., 1996; Babin et al., 2003b; Binding et al., 2008). Babin and Stramski (2004) reported that absorption by minerogenic particle populations (a_m) was largely attributable to the content of iron (Fe). Recently, advancements have been made in estimating the minerogenic scattering coefficient (b_m) based on an individual particle analysis technique that provides both morphological and chemical characterizations (Scanning electron microscopy interfaced with Automated image and X-ray analyses (SAX)), coupled with forward Mie theory-based calculations (Peng and Effler, 2007; Peng et al., 2007, 2009). The integrated SAX–Mie theory approach also represents a basis to directly estimate a_m, mediated through the imaginary (absorption) part of the refractive index (Wozniak and Stramski, 2004).

Lake Superior has been described as an optically complex system that represents a challenge for robust remote sensing of water quality (Li et al., 2004). Partitioning of a into a_x contributions for visible wavelengths for multiple sites has not been reported for this lake. Minerogenic particles, mostly clay minerals in the 1–10 μm size range, were found to be an important component of backscattering in eastern Lake Superior and Keweenaw Bay in July of 2006 (Peng et al., 2009). Rigorous partitioning of a according to a_x and establishment of relationships between a_x and concentrations of optically active constituents have been recommended for the lake to support remote sensing initiatives (Gons and Auer, 2004; Gons et al., 2008). This paper documents spectral characteristics, spatial patterns, and relationships with optically active constituents for a_x for Lake Superior and Keweenaw Bay based on surveys in 2006 and 2007. The results are considered in the context of the modest literature that describes a_x for lacustrine systems and other case 2 waters, and remote sensing issues for the lake. Symbols and abbreviations adopted in the paper (Table 1) are consistent with those used by the optics research community. Particular attention is given to the role of minerogenic particles and their Fe content in influencing a_{NAP}, based on paired SAX results (Peng et al., 2009) and Mie theory calculations.

Table 1
Abbreviations and symbols.

Abbreviations	
AOPs	Apparent optical properties; those that depend on the underwater light field
CDOM	Colored dissolved organic material
Chl	Chlorophyll *a*
DOC	Dissolved organic carbon
FeXRI	Iron X-ray relative intensity (%)
FSS	Fixed, or inorganic, suspended solids
NAP	Non-algal particles
PAV_m	Projected area concentration of minerogenic particles (m^{-1})
SAX	Scanning electron microscopy interfaced with automated image and X-ray analyses
TSS	Total suspended solids
VSS	Volatile (organic) suspended solids
XRI	X-ray relative intensity (%)
Symbols	
$a(\lambda)$	Total spectral absorption coefficient (m^{-1}), wavelength (λ) sometimes omitted
$a_x(\lambda)$	Spectral absorption coefficient for component "x" (m^{-1}); "x" (as subscript) can be CDOM, NAP, detritus (d), particles (p), minerogenic particles (m), phytoplankton (φ), and water (w)
$\hat{a}_x(\lambda_r)$	*a* for component "x" (CDOM or NAP) at reference wavelength λ_r (m^{-1})
$a^*_{CDOM,DOC}(440)$	DOC-specific a_{CDOM} at $\lambda = 440$ nm ($m^2\ g^{-1}$)
$a^*_{NAP,TSS}(440)$	TSS-specific a_{NAP} at $\lambda = 440$ nm ($m^2\ g^{-1}$)
$a^*_{NAP,FSS}(440)$	FSS-specific a_{NAP} at $\lambda = 440$ nm ($m^2\ g^{-1}$)
$a^*_{p,TSS}(440)$	TSS-specific a_p at $\lambda = 440$ nm ($m^2\ g^{-1}$)
$a^*_{\varphi,Chl}(440)$	Chl-specific a_φ at $\lambda = 440$ nm ($m^2\ g^{-1}$)
$a^*_{\varphi,Chl}(676)$	Chl-specific a_φ at $\lambda = 676$ nm ($m^2\ g^{-1}$)
b_m	Scattering coefficient for minerogenic particles (m^{-1})
d_j	Size of minerogenic particle *j* (μm)
m	Relative (to water) complex refractive index
n	Real part of m
n'	Imaginary part of m
N_m	Number of minerogenic particles per unit volume of water (number·m^{-3})
$PA_{m,j}$	Projected area of minerogenic particle *j*
$Q_{am,j}$	Absorption efficiency factor for minerogenic particle *j*
S_{CDOM}	Slope of the $a_{CDOM}(\lambda)$ spectrum (nm^{-1})
S_{NAP}	Slope of the $a_{NAP}(\lambda)$ spectrum (nm^{-1})
V	Water sample volume for SAX (m^{-3})
λ_r	Reference wavelength of light (nm)

Methods

Study sites

This study is based on analysis of samples collected in two surveys conducted in July (5–14) 2006 and August (18–24) 2007. The 2006 survey included 11 sites extending from the mouth of the Sturgeon River in the Portage Lake portion of the Keweenaw Waterway (KW0), down to the waterway's exit into Keweenaw Bay (KW1), along the primary axis of the bay (KB1–KB6), and out into eastern Lake Superior (three sites, ELS1–ELS3; Fig. 1). Site designations (except KW0) are those used by Peng et al. (2009). The bay is 36 km long, with widths ranging from 3 to 18 km. The bay sites represent a subset of the twelve included in a study of its intrinsic water color (Gons and Auer, 2004). The Sturgeon River has been described as humic (Ma and Green, 2004) and highly stained (Gons and Auer, 2004). This river is the largest tributary entering the bay, with an average annual flow rate of 26 $m^3\ s^{-1}$.

The 2007 survey included nine sites (Fig. 1) that represent a subset of those monitored in USEPA's long-term program (GLNPO, 2009). Site designations for the 2007 samples correspond to those used in that monitoring program.

Measurements

Near-surface (within upper 2 m) samples were collected and processed the day of collection for subsequent laboratory analyses. Measurements of concentrations of optically active substances were conducted on sample aliquots for total (TSS; Whatman 934-AH, 1.5 μm pore size) and fixed (FSS, after 550 °C; i.e., inorganic) suspended solids (Clesceri et al., 1998), dissolved organic carbon (DOC) (Clesceri et al., 1998; for 2007 samples only), and chlorophyll *a* (Chl; Parsons et al., 1984).

The methods for optical measurements generally tracked those specified for satellite ocean color calibration/validation activities (Mitchell et al., 2003). Determinations of a_{CDOM}, a_{NAP}, and a_ϕ were made on samples from 2006, while measurements were limited to a_{CDOM} in 2007. Lake water was filtered under low vacuum on pre-rinsed (deionized water) 0.2 μm pore size Millipore membranes for CDOM absorption measurements and refrigerated (4 °C) in the dark until analyzed. Absorbance of the filtered water was measured in a 10 cm quartz cuvette from 400 to 700 nm at 2 nm increments with a dual beam spectrophotometer (Perkin Elmer, Lambda 40), with deionized water used as the reference. A baseline correction was made by subtracting the absorbance value averaged over a 14 nm interval around 693 nm from all the spectral values. These spectra were described according to

$$a_{CDOM}(\lambda) = \hat{a}_{CDOM}(\lambda_r)e^{(-S_{CDOM}(\lambda-\lambda_r))} \quad (2)$$

where λ_r (nm) is the reference wavelength, $\hat{a}_{CDOM}$ (λ_r) is the CDOM absorption at λ_r, and S_{CDOM} (nm^{-1}) is the slope of the a_{CDOM} (λ) spectrum. Values of S_{CDOM} were estimated through a nonlinear

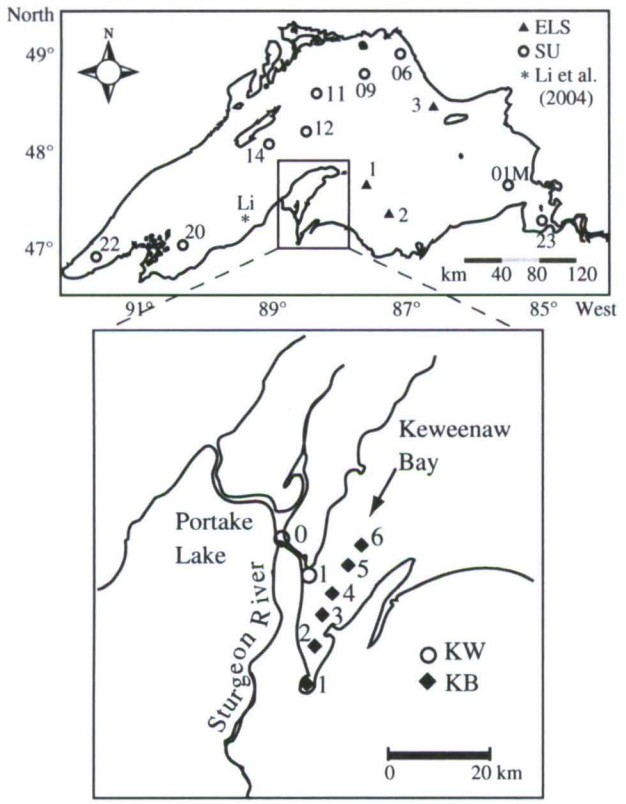

Fig. 1. Map of Lake Superior with sampling sites in the Sturgeon River (KW0) and its inflow zone (KW1), Keweenaw Bay (KB, 6 sites), eastern Lake Superior (ELS, 3 sites, 2006), and lake-wide (SU, 9 sites, 2007). Site monitored by Li et al. (2004) is also shown.

regression fitting approach (Twardowski et al., 2004) for the exponential function (Eq. (2), with $\lambda_r = 440$ nm) over the 400 to 500 nm wavelength interval (Perkins et al., 2009, 2010). It should be noted that this fitting method differs from that of taking the logarithm of a_{CDOM} absorption and obtaining S_{CDOM} as the slope from a linear least-squares fit (Twardowski et al., 2004).

Water samples were filtered onto 25 mm diameter glass fiber filters (Whatman GF/F, nominal pore size of 0.7 μm) at low vacuum for particle absorption measurements. Filters were stored in opaque containers in the dark and refrigerated until analyzed. The absorption spectrum of particles retained on the filters, $a_p(\lambda)$, was determined using the method of Lohrenz (2000). Particle absorbance was measured between 400 and 750 nm at 2 nm increments using a dual beam spectrophotometer equipped with a 100 mm integrating sphere (Perkins Elmer, Lambda 18). Correction for path length amplification was made using the relationship developed by Cleveland and Weidemann (1993). $a_{NAP}(\lambda)$ was measured after pigment bleaching with sodium hypochlorite (Ferrari and Tassan, 1999). The final determinations of $a_p(\lambda)$ and $a_{NAP}(\lambda)$ were made by subtracting the average of measured values over the 740 to 750 nm range from the spectral observations. The phytoplankton absorption spectrum, $a_\phi(\lambda)$, was obtained through a residual calculation

$$a_\varphi(\lambda) = a_p(\lambda) - a_{NAP}(\lambda) \tag{3}$$

This determination of $a_\phi(\lambda)$ includes absorption by all pigments bleached by sodium hypochlorite. The a_{NAP} spectra were described in an analogous manner to a_{CDOM} according to

$$a_{NAP}(\lambda) = \hat{a}_{NAP}(\lambda_r) e^{(-S_{NAP}(\lambda-\lambda_r))} \tag{4}$$

where $\hat{a}_{NAP}(\lambda_r)$ is NAP absorption at λ_r (440 nm), and S_{NAP} is the slope of the $a_{NAP}(\lambda)$ spectrum. Values of S_{NAP} were estimated through the same nonlinear regression fitting approach used for S_{CDOM} for the exponential function (Eq. (4), with $\lambda_r = 440$ nm) for data from 482 to 618 nm and 712 to 750 nm (Babin et al., 2003b). The exclusion of 400–480 and 620–710 nm ranges avoids the potential effects of residual pigment absorption that may have persisted after the sodium hypochlorite treatment (Babin et al., 2003b).

SAX data and absorption by minerogenic particles

Results from SAX characterizations of the 2006 samples, in the context of light-scattering implications, were reported by Peng et al. (2009). The details of sample preparation and instrumentation methodology for SAX have been described elsewhere (Peng and Effler, 2005, 2007). Approximately 2000 individual particles were analyzed for each sample for both composition and morphology characteristics (Peng et al., 2009). SAX provided information on chemical composition, number concentration, and size distribution of minerogenic particles for forward estimates of both b_m and a_m.

Composition of individual minerogenic particles is represented by the X-ray relative intensities (XRI, in percentage) of 16 elements [including aluminum (Al), silica (Si), calcium (Ca), and iron (Fe)]. Based on composition, particles were classified into five predefined generic types: clay, quartz, silica (Si)-rich, calcium (Ca)-rich, and miscellaneous (Peng et al., 2009). The projected area of minerogenic particles per unit volume of sample (PAV_m), determined with SAX (Peng and Effler, 2007), is a fundamental attribute of the light-attenuating properties of these particles (Peng and Effler, 2007; Peng et al., 2009). The minerogenic particle populations of the 2006 survey were dominated by clay minerals, representing on average 72% of the total PAV_m at each of the sites (Table 2). Such particles have terrigenous origins (Peng et al., 2009).

The SAX–Mie theory calculation approach was used here to make forward estimates of a_m based on the same individual particle characterizations, according to

$$a_m(\lambda) = \frac{1}{V}\sum_{j=1}^{N_m} Q_{am,j}\left(n', \lambda, d_j\right) PA_{m,j} \tag{5}$$

where V is the water sample volume, N_m is the number of minerogenic particles per unit volume of water, $Q_{am,j}$ is the absorption efficiency factor (determined from Mie theory calculations; Bohren and Huffman, 1983) for minerogenic particle j, n' is the imaginary portion of the complex refractive index ($m = n - in'$, where n the is the real portion), λ is the wavelength, d_j is the size of particle j, and $PA_{m,j}$ is the projected area of minerogenic particle j. Values of n' are more uncertain than those for n (Wozniak and Stramski, 2004). The relationship between minerogenic particles and a_{NAP} was investigated in two ways: (1) empirically, through regression analyses between a_{NAP} and PAV_m and a_{NAP} and average FeXRI of minerogenic particles (not reported by Peng et al. (2009)), and (2) mechanistically, through a series of Mie theory calculations of $a_m(440)$ based on the paired SAX data (Peng et al., 2009). Various cases of n' were adopted in the Mie theory calculations that included the approach to equivalence (i.e.,

Table 2
Summary of average minerogenic particle chemistry according to five classes, in the context of contributions to PAV_m.

Chemical class	Average contribution (%)	n'
Clay	72.3	4 scenarios[a]
Quartz	7.7	0.0002
Si-rich	10.2	4 scenarios
Ca-rich	3.0	0.0002
Miscellaneous	6.9	4 scenarios

[a] $n' = 0.003, 0.006, 0.008, 0.010$.

closure) with a_{NAP}. The adopted n' values were guided by the related, albeit limited, literature (Patterson et al., 1977; Wozniak and Stramski, 2004). Values of n' were assumed to be equal for the clay, Si-rich, and miscellaneous particle classes for the various cases of n', while the quartz and Ca-rich classes had much lower values that were held constant (Table 2; Wozniak and Stramski, 2004).

Results

Spectral characteristics

Representative spectra for the three measured components (a_x) are illustrated for site KB3 (Fig. 2, note scale changes for a_x). Exponential decreases with increasing wavelength were observed for a_{CDOM} (Fig. 2a) and a_{NAP} (Fig. 2b). The non-linear regression fits generally performed well in representing these spectra over the designated calculation wavelength intervals for the slope values (Fig. 2a and b). All phytoplankton spectra demonstrated two maxima, a broad one at ~440 nm and the other better defined at 676 nm (Fig. 2c). Instrument noise was apparent for both a_{NAP} (Fig. 2b) and a_ϕ (Fig. 2c) spectra because of the relatively low absorption signals for these components associated with their low concentrations.

The S_{CDOM} values for KW0 and KW1 were the highest of the 2006 survey, though these were approached by the observation for KB1 (Table 3). Values for the lake and bay sites were in the range of 0.0111–0.0160 nm^{-1}; the mean for these sites was 0.0126 nm^{-1}, the coefficient of variation (cv) was 11%. The mean S_{NAP} for these sites was similar, 0.0131 nm^{-1} (cv = 13%). Significant relationships between S_{CDOM} and a_{CDOM}, and S_{NAP} and a_{NAP}, were not observed for the lake and bay sites.

Values of S_{CDOM} for the lake sites of the 2007 survey (Table 4) were generally similar to those of the KB and ELS sites of 2006 (Table 3). The 2007 observations were in the range of 0.0089 (SU23) to 0.0139 nm^{-1} (SU22) for all sites, with an average of 0.011 nm^{-1} (cv = 14%). a_ϕ spectra were characterized by the ratio of the blue (λ = 440 nm) to red (λ = 676 nm) peaks (Table 3, e.g., Babin et al., 2003b; Perkins et al., 2010). All but one of the ratio values were in the range of 2.06–3.19, with an average of 2.54 (cv = 23%) excluding site KB3 (4.24).

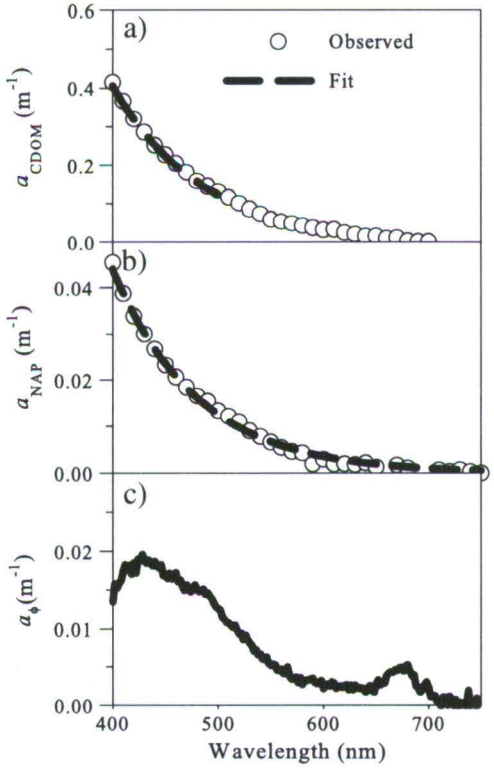

Fig. 2. Representative spectra for light absorbing components for site KB3: (a) a_{CDOM}, with fit, (b) a_{NAP}, with fit, and (c) a_ϕ. Note scaling difference for a_x.

Absorption by components

Spatial patterns of a_x are described for λ = 440 nm, the commonly adopted blue reference wavelength (Kirk, 1994). Values of a_{CDOM} (440) decreased in a generally progressive manner from the Sturgeon River to the open waters of the lake in the 2006 survey, according to river>inflow mixing zone>bay>eastern Lake Superior (Fig. 3a, note scale change for a_x), though substantial spatial variability was manifested (Table 5). On average, the KB site levels were 70% higher than the ELS sites. Though a_{NAP}(440) levels were substantially lower, a similar spatial pattern was observed (Table 5, Fig. 3b). The river a_{NAP} (440) value exceeded the inflow mixing zone level by more than 2-fold, which in turn was about 6-fold greater than the bay, and the bay was about 2-fold higher than for the ELS sites. The spatial pattern for a_ϕ differed in that average values for the KB and ELS sites were nearly equal (Fig. 3c). The spatial pattern of a(440) (Fig. 3d), determined from the summation of a_x (Eq. (1)), generally tracked that of a_{CDOM} (440) (Fig. 3a), the dominant absorbing component.

a_{CDOM}(440) represented ≥75% of a(440) at all sites. a_{CDOM}(440) was 80% of a(440) for KW0, 77% for KW1, 81% for the average of the KB sites, and 75% for the average of the ELS sites (Fig. 3e). NAP was the second largest component for KW0 (12%) and KW1 (13%), but was less than a_ϕ at the KB (7 vs. 9%) and ELS (9 vs. 13%) sites. a_w(440) was the smallest component at all sites; its greatest contribution was where a(440) was the lowest (3%, on average, based on observations for ELS sites). The general spatial pattern of the spectral contributions of a_x is illustrated based on observations for KW0 (Fig. 4a), KW1 (Fig. 4b), KB4 (Fig. 4c), and ELS2 (Fig. 4d). The fractional contribution (Fig. 4) format serves to contrast the spatial differences as well as depict challenges faced in resolution of the signals from the various components, particularly a_ϕ. a_w was dominant for λ>600 nm. This dominance was manifested at lower wavelengths as the other components of a decreased. The contributions a_{NAP} and a_ϕ were spectrally relatively featureless at KW0 and KW1 (Fig. 4a and b) because of the high a_{CDOM}, though the a_ϕ component was apparent for KB4 and ELS2 at λ<500 nm, representing about 12 and 20% of a at these maxima. a_ϕ was larger than a_{NAP} and a_{CDOM} at its secondary peak (λ = 676 nm) at all sites, but its contribution to a at this wavelength was small compared to a_w. The contribution of a_w at λ = 676 nm was more than 6-fold greater than a_ϕ at KW0, 17-fold at KW1, 53-fold at KB4, and 40-fold at ELS2.

Optically active constituents and relationships with a_x

The highest Chl in the 2006 survey was in the Sturgeon River (KW0) (Table 3). The concentration at KW1 was about 58% lower, but more than 3-fold higher than the bay concentrations. Chl levels were higher at the ELS sites than those at the KB sites, about 32% on average. TSS and FSS concentrations were distinctly higher for KW0 and KW1 than the bay sites (Table 3). The suspended solids data for the bay sites are uncertain because of the low weights accumulated on the filters in the analyses, and are considered applicable only on a bay-average basis. No suspended solids measurements were available for the ELS sites. The PAV_m data are those reported by Peng et al. (2009), except for KW0 (not previously reported). A distinct gradient in this metric of minerogenic particles was manifested, according to Sturgeon River>inflow mixing zone>bay>ELS sites. The FeXRI data presented here (Table 3) from SAX were not reported in previous work. The highest FeXRI values were in the Sturgeon River and its inflow mixing zone. A gradient prevailed in the bay, with decreases manifested with the approach to the open waters. The levels of FeXRI

Table 3
Optically active constituent concentration and spectral characteristics, 2006 survey.

	Chl ($mg\,m^{-3}$)	*TSS* ($g\,m^{-3}$)	*FSS* ($g\,m^{-3}$)	PAV_m (m^{-1})	*FeXRI*	$\frac{FeXRI}{PAV_m}$	S_{CDOM} (nm^{-1})	S_{NAP} (nm^{-1})	$\frac{a_\phi(440)}{a_\phi(676)}$
KW0	3.85	1.93	0.93	0.24	8.8	36	0.0169	0.0120	2.083
KW1	1.63	1.43	1.03	0.182	9.4	52	0.0168	0.0118	2.920
KB1	0.48	0.30	0.10	0.067	6.3	94	0.0160	0.0144	2.540
KB2	0.54	0.24	0.04	–	–	–	0.0125	0.0125	3.187
KB3	0.42	0.28	0.07	0.080	6.2	78	0.0119	0.0125	4.243
KB4	0.45	0.63	0.33	0.030	5.3	177	0.0117	0.0105	2.852
KB5	0.48	0.30	0.12	0.043	4.1	95	0.0111	0.0131	2.457
KB6	0.43	0.37	0.17	0.050	4.0	80	0.0126	0.0165	2.180
ELS1	0.69			0.016	4.1	256	0.0117	0.0128	2.550
ELS2	0.57			0.026	4.4	169	0.0127	0.0121	2.531
ELS3	0.81			0.022	4.0	181	0.0135	0.0135	2.063
Mean	0.94	0.69	0.35	0.076	5.7	122	0.0134	0.0123	2.691
Std. dev.	1.02	0.64	0.40	0.075	2.0	70.1	0.002	0.0016	0.623

were nearly equal for KB5, KB6, and the ELS sites (Table 3). The relative iron content of the minerogenic particles (e.g., on a projected area basis, indicated by the ratio FeXRI ÷ PAV_m; Table 3), generally increased from the river to the bay, and from the bay to ELS sites. Concentrations of DOC were in the narrow range of 1.3–1.5 g m^{-3} for the 2007 survey of Lake Superior (Table 4).

Relationships between a_x and optically active constituents were evaluated as "specific" absorption coefficients, which have been normalized by the constituent concentration of interest (e.g., Binding et al., 2008). These relationships support comparison to values of specific absorption coefficients reported for other systems. The average Chl-specific a_φ for $\lambda = 440$ ($a^*_{\phi,Chl}(440)$) and 676 nm ($a^*_{\phi,Chl}(676)$) for the 2006 cruise, excluding KW0 and KW1, were 0.046 and 0.017 $m^2\,mg^{-1}$, respectively; the corresponding values of cv were 26 and 36%. The average $a^*_{\phi,Chl}(440)$ for the KB sites (0.050 $m^2\,mg^{-1}$) was significantly ($p<0.001$) higher than the ELS sites (0.037 $m^2\,mg^{-1}$). Average specific absorption coefficients for NAP are presented based on both TSS and FSS, because of: (1) the ambiguity associated with the inclusion of phytoplankton biomass within the TSS measurement, and (2) the uncertainty concerning the relative roles of minerogenic versus detrital particles in regulating a_{NAP}. The average specific absorption coefficient values for NAP based on TSS ($a^*_{NAP,TSS} = a_{NAP}(440) \div TSS$) for KB and KW sites were 0.057 (cv = 57%) and 0.10 $m^2\,g^{-1}$, respectively. The corresponding specific absorption coefficient values for NAP based on FSS ($a^*_{NAP,\,FSS} = a_{NAP}(440) \div FSS$) were 0.083 (cv = 39%) and 0.27 $m^2\,g^{-1}$. The relationship between a_p ($a_\phi + a_{NAP}$) and TSS does not suffer from the above ambiguities. The average specific absorption coefficients for overall particle absorption ($a^*_{P,TSS} = a_p(440) \div TSS$) for the KB and KW sites were 0.13 (cv = 36%) and 0.17 $m^2\,g^{-1}$, respectively. The average specific absorption coefficient for DOC for $\lambda = 440$ nm ($a^*_{CDOM,DOC}(440) = a_{CDOM}(440) \div DOC$) based on paired measurements for the 2007 cruise was 0.10 $m^2\,g^{-1}$ (cv = 37%).

Table 4
DOC concentrations, S_{CDOM}, a_{CDOM} and $a_{CDOM}(440) \div DOC$, 2007 survey.

	DOC ($g\,m^{-3}$)	S_{CDOM} (m^{-1})	$a_{CDOM}(440)$ (m^{-1})	$\frac{a_{CDOM}(440)}{DOC}$ ($m^2\,g^{-1}$)
SU1	1.3	0.0108	0.119	0.092
SU6	1.5	0.0107	0.109	0.073
SU9	1.3	0.0103	0.145	0.112
SU11	1.3	0.0115	0.132	0.101
SU12	1.3	0.0105	0.150	0.115
SU14	1.4	0.0135	0.073	0.052
SU20	1.4	0.0098	0.208	0.148
SU22	1.5	0.0139	0.157	0.105
SU23	1.4	0.0090	0.234	0.167
Mean	1.4	0.0107	0.145	0.105
Std. dev.	0.083	0.0016	0.049	0.035

Minerogenic particles, a_{NAP}, and a_m

PAV_m was a strong predictor of a_{NAP} for the KB and ELS sites of the 2006 survey, explaining 69% of the variability according to linear least

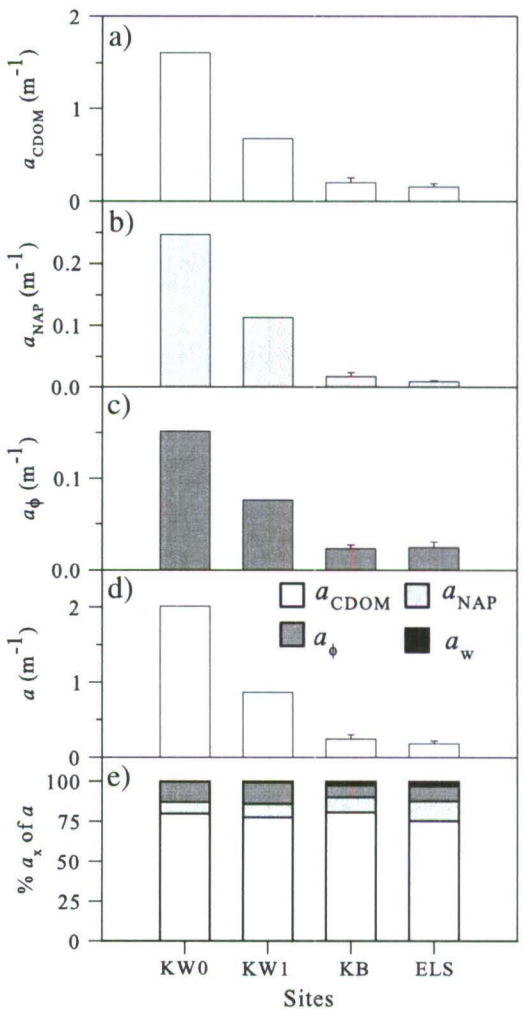

Fig. 3. Spatial patterns of $a_x(440)$ for 2006 survey, with mean and standard deviation (vertical bars) values for KB and ELS sites: (a) a_{CDOM}, (b) a_{NAP}, (c) a_ϕ, (d) a, by summation of a_x, and (e) contributions of a_x. Note scaling difference for a_x and a in (a)–(d).

Table 5
Values of a_x and relationships with optically active constituents, as ratios, for 2006 survey.

	$\frac{a_{CDOM}(440)}{(m^{-1})}$	$\frac{a_{NAP}(440)}{(m^{-1})}$	$\frac{a_{NAP}(440)}{TSS}$ $(m^2\,g^{-1})$	$\frac{a_{NAP}(440)}{FSS}$ $(m^2\,g^{-1})$	$\frac{a_P(440)}{TSS}$ $(m^2\,g^{-1})$	$\frac{a_\phi(440)}{(m^{-1})}$	$\frac{a_\phi(676)}{(m^{-1})}$	$\frac{a_\phi(440)}{Chl}$ $(m^2\ mg^{-1})$	$\frac{a_\phi(676)}{Chl}$ $(m^2\ mg^{-1})$
KW0	1.607	0.247	0.1279	0.2472	0.2065	0.152	0.073	0.0395	0.0190
KW1	0.674	0.113	0.0791	0.2833	0.1325	0.077	0.026	0.0470	0.0161
KB1	0.180	0.020	0.0673	0.1010	0.1558	0.027	0.010	0.0553	0.0218
KB2	0.267	0.022	0.0928	0.1113	0.1843	0.022	0.007	0.0407	0.0128
KB3	0.252	0.027	0.0942	0.1232	0.1602	0.019	0.004	0.0445	0.0105
KB4	0.186	0.016	0.0249	0.0525	0.0629	0.024	0.008	0.0535	0.0188
KB5	0.218	0.009	0.0302	0.0518	0.0959	0.020	0.008	0.0411	0.0167
KB6	0.173	0.011	0.0308	0.0572	0.1064	0.028	0.013	0.0653	0.0299
ELS1	0.183	0.010				0.018	0.007	0.0263	0.0103
ELS2	0.105	0.0065				0.029	0.011	0.0504	0.0199
ELS3	0.155	0.0104				0.027	0.013	0.0331	0.0161
Mean	0.186	0.016	0.0732	0.106	0.1441	0.027	0.010	0.0445	0.0167
Std. dev	0.439	0.073	0.037	0.089	0.0479	0.041	0.020	0.0109	0.0056

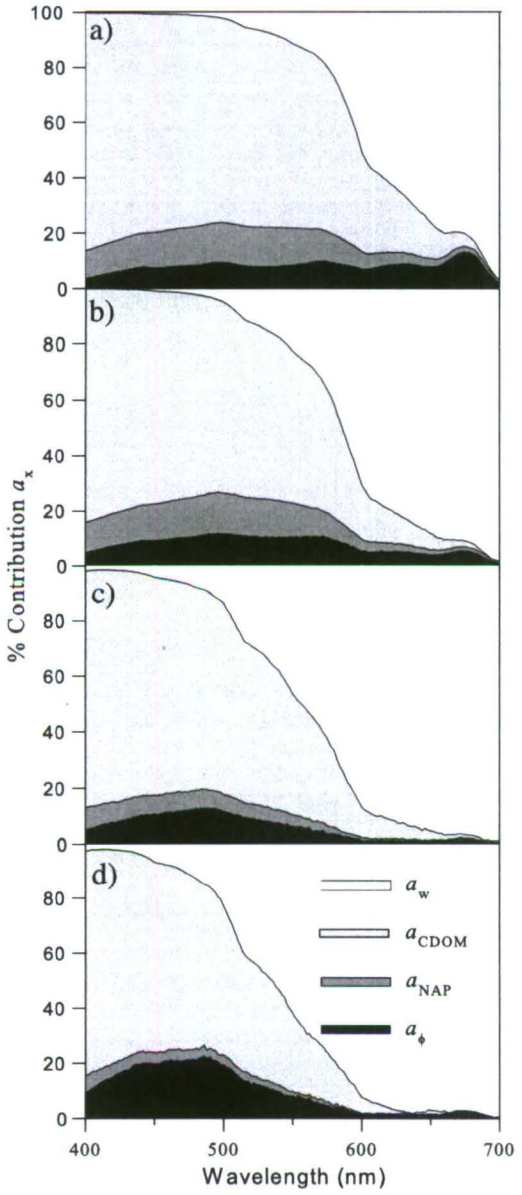

Fig. 4. Spectral contributions (%) of a_x to a for selected sites: (a) KW0, (b) KW1, (c) KB4, and (d) ELS2.

squares regression (Fig. 5a; $p<0.01$). Inclusion of the river and inflow zone sites (see inset, Fig. 5a) results in a stronger relationship, but this is an artifact of the disproportionate effect of their much higher values. Higher a_{NAP} per unit PAV_m is indicated for these KW sites. The relationship between a_{NAP} and FeXRI for the KB and ELS sites was somewhat stronger (Fig. 5b; $r^2=0.82$, $p<0.01$).

The relationship between the Mie theory estimates of $a_m(440)$ for $n'=0.008$ and PAV_m is presented (Fig. 5c) with a linear least squares regression fit, along with fits for $a_m(440)$ calculations for the other n' values considered (0.003, 0.006, 0.010). The estimates of a_m are shown to be approximately linearly related to PAV_m for all samples ($r^2=0.97$, $p<0.01$) and when KW0 and KW1 are not considered (inset of Fig. 5c; $r^2=0.62$, $p=0.02$). Moreover, a_m increases in a non-linear manner as n' increases (Fig. 5c). The relationship between $a_{NAP}(440)$ and the $a_m(440)$ estimates is depicted for the scenario of $n'=0.008$ (Fig. 5d). According to this scenario $a_m(440)$ would represent on average 84% of $a_{NAP}(440)$. About 40% of the variability in $a_{NAP}(440)$ was explained by the independent estimates of $a_m(440)$ for $n'=0.008$ ($p=0.10$). For the $n'=0.006$ case (not shown), $a_m(440)$ estimates represented on average about 79% of $a_{NAP}(440)$. Positive y-intercept values were obtained for all scenarios that converged at a value of about 0.006 m^{-1}, though these were not significantly different from zero.

Discussion

Spectral characteristics

The slopes of the CDOM and NAP absorption spectra, S_{CDOM} and S_{NAP}, are generally considered to be proxies of the composition of contributing constituents (Babin et al., 2003b). S_{CDOM} has been used to correct remote sensing bio-optical data (Schwarz et al., 2002). Changes in S_{CDOM} have been attributed to differences in CDOM composition, sources and sinks (Helms et al., 2008), and changes in molecular weight of fulvic acids (Carder et al., 1989; Blough and Green, 1995). Both increases (Vodacek et al., 1997; Del Vecchio and Blough, 2004) and decreases (Morris and Hargreaves, 1997) in S_{CDOM} from photodegradation have been reported.

The variety of protocols adopted to estimate S_{CDOM} from measured spectra has made comparison of results from different studies difficult, as the effects are large relative to the real differences that may be attributable to differences in CDOM composition (Twardowski et al., 2004; Helms et al., 2008; Loiselle et al., 2009). The two primary sources of variability associated with these protocols are the wavelength interval considered and the calculation method adopted (Twardowski et al., 2004). Narrow wavelength intervals (e.g., 100–150 nm widths) have advantages (Helms et al., 2008) and have

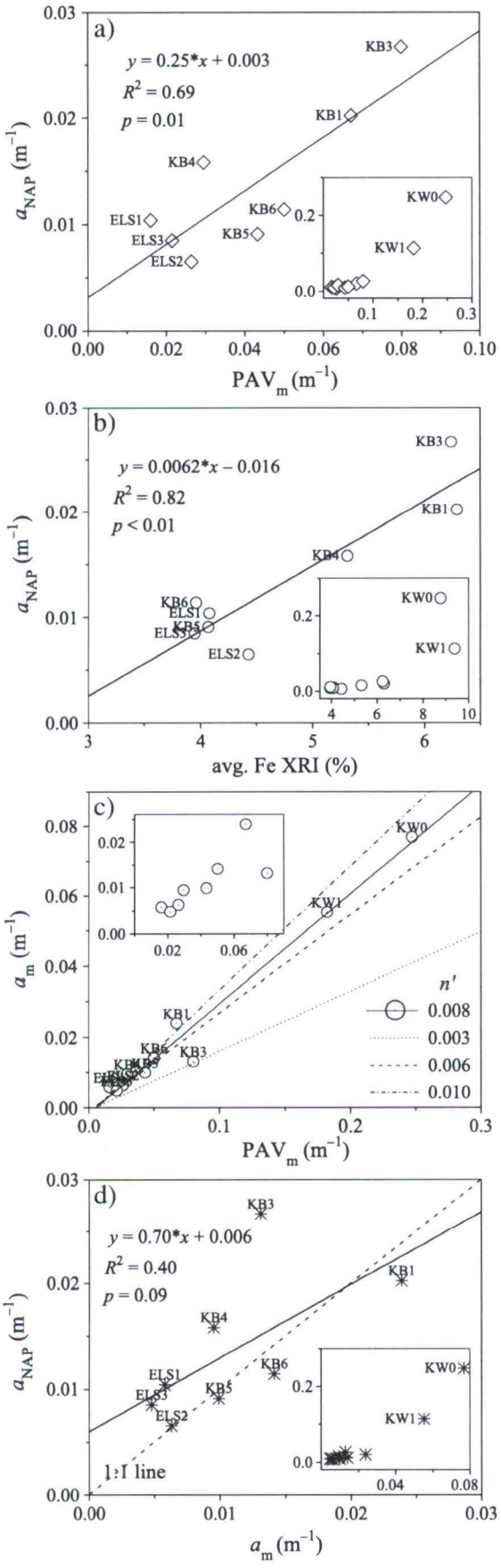

generally been adopted in recent studies (Babin et al., 2003b; Binding et al., 2008; Perkins et al., 2009, 2010). Some modest deviations in the wavelength specifications persist, though their effects are probably minor; e.g., 350–500 nm by Babin et al. (2003a), 350–440 nm by Binding et al. (2008), and 400–500 nm by Perkins et al. (2009, 2010; and adopted here). A unification of calculation protocols appears to have evolved recently that supports the adopted non-linear regression fitting approach (Babin et al., 2003b; Twardowski et al., 2004; Perkins et al., 2009, 2010).

Most of the S_{CDOM} observations for the bay and Lake Superior (Tables 2 and 3) were at or slightly below the lower bounds of the populations reported elsewhere. A single a_{CDOM} spectrum (S_{CDOM}~0.011) presented by Li et al. (2004; fig. 8, p. 454) from a site (Fig. 1) in west central Lake Superior (1999 collection) is consistent with our observations (Tables 2 and 3). The mean of our bay and main lake observations for the 2006 survey (0.0126 nm^{-1}) and the average for the 2007 survey (0.011 nm^{-1}) were lower than those reported for other systems to date; e.g., 0.0176 nm^{-1} for European coastal waters (Babin et al., 2003b), 0.0161 nm^{-1} for Lake Erie (Binding et al., 2008), 0.0168 nm^{-1} for Onondaga Lake, NY (90 observations, Perkins et al., 2010), 0.0141–0.0186 nm^{-1} for the 11 Finger Lakes of New York (Perkins et al., 2010). The variability among sites encountered for this attribute in this study, cv = 14%, was similar to that reported by Babin et al. (2003a) (cv = 11.4%) for European coastal waters. The generally low values of S_{CDOM} obtained suggest an atypical composition for CDOM in this system. An unusually large contribution of high molecular weight humic acids, relative to the lower molecular weight fulvic acids, is one consistent (Carder et al., 1989) potential explanation. Some of the greatest deviations from the mean were observed for near-shore locations (e.g., KB1, Table 3; SU22 and SU23 Table 4), suggesting local differences in CDOM composition. Binding et al. (2008) reported even greater spatial variations in S_{CDOM} in Lake Erie based on 90 observations.

The S_{CDOM} value for the humic-rich Sturgeon River was higher than the ELS sites and most of the KB sites (Table 3; but similar to five other tributaries to Lake Superior sampled in April 2009, unpublished data, Upstate Freshwater Institute), counter to expectations based on photoirradiation effects on lake CDOM and system-specific slopes reported by Ma and Green (2004), albeit for a different wavelength range (230–400 nm). Their river value (0.0144 nm^{-1}) was similar to our observation (0.0169 nm^{-1}). However, their slope value for lake water, 0.0259 nm^{-1}, was much higher than reported here for S_{CDOM} and other systems where longer (visible) wavelength ranges were considered, suggesting an effect of the different wavelength intervals considered.

S_{NAP} has received far less attention; for example, values have been reported in only a limited number of studies of lacustrine systems (Binding et al., 2008; Perkins et al., 2009, 2010). The S_{NAP} values reported here (mean of 0.0129 nm^{-1}) are similar to those reported elsewhere, where the same wavelength and calculation protocols were used. Babin et al. (2003a) reported a mean of 0.0123 nm^{-1} (cv = 11%). Perkins et al. (2009) reported an overall mean of 0.0121 for the Finger Lakes of New York, with means for the individual lakes in the range of 0.0113–0.0126 nm^{-1}. The mean for Onondaga Lake was 0.0126 nm^{-1} (Perkins et al. 2010). The mean for Lake Erie was reported to be somewhat lower (0.011 nm^{-1}, Binding et al., 2008). However, the wavelength interval and calculation protocols were not specified for the Lake Erie observations. The a_{NAP} spectra reported here had shapes (Fig. 2b) that were also generally similar to those described for natural minerogenic particle assemblages that have been attributed to the effects of iron content (Babin and Stramski, 2004).

Fig. 5. Evaluations of relationships related to minerogenic particles and a_{NAP}, with linear least-squares regression statistics: (a) a_{NAP} versus PAV_m, (b) a_{NAP} versus average FeXRI, (c) a_m versus PAV_m, and (d) a_{NAP} versus a_m. Insets include KW0 and KW1, except for (c).

Binding et al. (2008) presented evidence that a fraction of NAP was bleached by the sodium hypochlorite treatment that obscured the 440 nm a_ϕ peak in Lake Erie samples at $a_{CDOM}(440)$ levels as low as 0.10 to 0.18 m^{-1}. The effect was greater as a_{CDOM} increased (Binding et al., 2008). There were no indications that this was a problem for resolution of a_ϕ spectra for Lake Superior and Keweenaw Bay, as the peaks at $\lambda = 440$ nm were well resolved in all samples (e.g., Fig. 2c). Moreover, the threshold of concern for $a_{CDOM}(440)$ for the effect to be manifested (Binding et al., 2008) was exceeded in most of the 2006 Lake Superior samples (Table 5). The values of the ratio $a_\phi(440) \div a_\phi(676)$ observed for the KB and ELS sites were well centered in the portion of the population of observations reported for European coastal waters with similar levels of Chl, with the exception of the highest ratio obtained at KB3 (Table 5). The high ratio for this sample is probably spurious reflecting the diminished accuracy of the $a_\phi(676)$ peak from instrumentation noise. Variations in spectral features, including $a_\phi(440) \div a_\phi(676)$, are most often attributed to differences in the packaging effects and accessory pigment content of phytoplankton, features that depend on community composition (Bricaud et al., 1995; Babin et al., 2003b).

a_x patterns and relationships with optically active constituents

The general spatial patterns of a_{CDOM}, a_{NAP}, and PAV_m in the 2006 survey are consistent with terrigenous sources of these constituents, though the details are doubtless subject to substantial variations. For example, Budd (2004) resolved extensive spring-time sediment plumes in the Keweenaw region of Lake Superior through satellite remote sensing. Gons and Auer (2004) reported similar variability in a_{CDOM} (440) (single wavelength measurements only within the bay) in a 2003 survey, though their values were shifted somewhat lower. The results of the 2007 survey, as well as those for the ELS sites in 2006, indicate noteworthy variations in a_{CDOM} also occur in the open waters of the lake. Binding et al. (2008) reported even greater spatial variability in Lake Erie, with a range of 0.08–0.75 m^{-1} for $a_{CDOM}(440)$, compared to 0.105–0.267 m^{-1} for Keweenaw Bay and Lake Superior sites reported here. The mean for the bay and Lake Superior sites observed in this study was 25% less than reported for Lake Erie (Binding et al., 2008). The partitioning of $a_x(440)$ based on the single set of spectra presented by Li et al. (2004; fig. 8, p.454) tracked closely that reported for the ELS sites (Table 5).

Comparisons of specific absorption coefficient values obtained for a_x here with the limited observations reported for other systems establish substantial differences, indicating the need for system-specific relationships to support mechanistic modeling goals. The average specific absorption coefficient for CDOM based on DOC ($a^*_{CDOM,\ DOC}(440) = 0.107\ m^2\ g^{-1}$) from the 2007 cruise was similar to the mean reported for Lake Erie (0.102 $m^2\ g^{-1}$, Binding et al., 2008). However, the range for Lake Superior (0.052–0.167 $m^2\ g^{-1}$) was narrower (0.035–0.306 $m^2\ g^{-1}$, Binding et al., 2008). The utility of DOC as an optically active constituent to which a_{CDOM} can be linked is limited. In particular, the fraction of DOC that absorbs light (CDOM) is subject to substantial differences between systems and temporal variations within individual systems (Morris and Hargreaves, 1997). a_{CDOM} and DOC were not significantly correlated for the paired observations of the 2007 survey, a common finding (e.g., Perkins et al., 2010). The $a^*_{CDOM,DOC}(440)$ was nearly 2-fold greater in Onondaga Lake, NY (Perkins et al., 2010). DOC was not included in the comprehensive survey of a_x in coastal waters around Europe (Babin et al., 2003b), likely in recognition of the disconnection between this aggregate measure and a_{CDOM}.

Specific absorption coefficient information for NAP for lacustrine systems is rare. The $a^*_{NAP,TSS}(440)$ and $a^*_{NAP,FSS}(440)$ values reported here are consistent with values reported elsewhere for cases of dominance of a_{NAP} by minerogenic particles in marine systems (Babin et al., 2003b; Babin and Stramski, 2004). The mean $a^*_{NAP,TSS}(440)$ value for the KB sites (0.057 $m^2\ g^{-1}$) was similar to that reported for Lake Erie (0.0403 $m^2\ g^{-1}$, Binding et al., 2008) and European coastal waters (0.041 $m^2\ g^{-1}$, Babin et al., 2003b), but less than for Onondaga Lake (0.090 $m^2\ g^{-1}$, Perkins et al., 2010). The mean $a^*_{NAP,FSS}(440)$ value for the bay (0.083 $m^2\ g^{-1}$) was ~35% lower than reported for Lake Erie (Binding et al., 2008), but was 2-fold lower than for Onondaga Lake (Perkins et al., 2010). The findings of Babin and Stramski (2004) and the FeXRI dependence reported here (Fig. 5b) suggest at least a portion of the differences in the specific absorption coefficient for NAP between studies may be due to differences in Fe content of suspended solids. The mean $a^*_{P,TSS}(440)$ for the bay (0.128 $m^2\ g^{-1}$) was ~45% lower than reported for Onondaga Lake (Perkins et al., 2010).

The average Chl-specific $a_\varphi(440)$ for the KB and ELS sites, $a^*_{\phi,Chl}(440) = 0.046\ m^2\ mg^{-1}$, was generally consistent with most of the reported values in both the marine (Bricaud et al., 1995; Babin et al., 2003b) and lacustrine literature (Bukata et al., 1991; Effler, 1996; Perkins et al., 2010). However, it was distinctly lower than recently reported for Lake Erie (0.086 $m^2\ mg^{-1}$, Binding et al., 2008). The average value for $a^*_{\phi,Chl}(676)$, 0.017 $m^2\ mg^{-1}$, was similar to that reported for Onondaga Lake (Perkins et al., 2010).

Minerogenic particles and a_{NAP}

Empirical analyses

The strong relationship between a_{NAP} and PAV_m for the KB and ELS sites (Fig. 5a) supports the position that terrigenous (Table 2) minerogenic particles, mostly clay minerals, were important in regulating the observed differences in that component of a. PAV_m has both system-specific and conceptual advantages over the gravimetric measure of minerogenic particles (FSS). PAV_m is a more sensitive and precise (Peng and Effler, 2007; Peng et al., 2009) metric than FSS in dilute systems such as Lake Superior. Moreover, particle projected area (e.g., PAV_m) is more fundamentally connected to the light attenuating properties of particles (Owen, 1974; Iturriaga and Siegel, 1989; Peng and Effler, 2007) than gravimetric representations.

The positive y-intercept (0.003 m^{-1}) of the a_{NAP}–PAV_m relationship is consistent with contributions from another component(s) to a_{NAP}, that is likely organic detritus (Babin et al., 2003b; Binding et al., 2008). a_{NAP} is expected to be well represented by a two component model

$$a_{NAP} = a_m + a_d \tag{6}$$

where a_d = absorption associated with particulate detritus.

The even stronger relationship between a_{NAP} and FeXRI (Fig. 5b) further supports the position that minerogenic particles were important in regulating the observed spatial differences in a_{NAP} among the KB and ELS sites. Using pure minerogenic specimens and an array of land-based natural deposits, Babin and Stramski (2004) reported Fe content was a primary driver of a_m. To the authors' knowledge, the results presented here for Lake Superior are the first support (Fig. 5b) for a potentially central role for Fe content of minerogenic particles in regulation of a_{NAP} based on analysis of water column samples. However, the possibility that the observed relationship is instead an artifact of a covarying factor cannot be discounted. Absorption by Fe has been associated with a combination of the effects of Fe adsorbed to particle surfaces and embedded as an impurity in crystal lattices, with spectral absorption shapes similar to a pure iron hydroxide suspension (Babin and Stramski, 2004). The potential for a non-linear relationship was indicated for our results by the negative y-intercept for the linear regression expression and the much higher a_{NAP} values for modest increases in FeXRI for the KW0 and KW1 samples (see inset, Fig. 5b). However, higher detritus concentrations at these two sites may also have contributed to the latter feature.

Uncertainty prevails with regards to the interplay between CDOM and absorption by particles in general (Binding et al., 2008), and minerogenic particles specifically (Gallegos and Neale, 2002). The extent to which this can modify the inherent absorption characteristics of mineral particles (e.g., increase the effective n') remains unresolved.

Mie theory estimates of a_m

The strong relationships between Mie theory estimates of a_m and measurements of PAV_m, illustrated for the case $n' = 0.008$ (Fig. 5c), supports the position that PAV_m can also serve as a surrogate metric for a_m, as well as for b_m (Peng and Effler, 2007). The variability in the relationship between $a_m(440)$ and PAV_m is attributable to differences in the particles size dependencies of these features, as well as modest variations in the contributions of the various chemical classes to the minerogenic particle populations of these samples (Table 2). Based on the limited literature (Patterson et al., 1977; Wozniak and Stramski, 2004), the scenarios of $n' = 0.006$ and 0.008 appear to be the most reasonable for the clay particles. For example, an n' value of approximately 0.007 was specified for $\lambda = 440$ nm in a spectrum (350–750 nm) adopted by Wozniak and Stramski (2004) in modeling the optical properties of mineral particles in seawater. Specification of much lower values for quartz and Ca-rich (e.g., calcite) particles, as adopted here (Table 2), is consistent with a_m measurements on pure samples (Babin and Stramski, 2004).

A rigorous test of optical closure of the forward estimates of $a_m(440)$, based on integration of individual particle information from SAX into Mie theory calculations, cannot be supported by this data set because a_d was not independently quantified (Eq. (2)). However, the relationship between $a_{NAP}(440)$ and these forward method estimates of $a_m(440)$, presented here (Fig. 5d) for the first time, depicts features of consistency that are encouraging for future SAX-based closure efforts and partitioning of a_{NAP} according to a_m and a_d. The level of consistency is impressive in the context of the multiple sources of uncertainty that could influence the results. First, the estimated magnitudes of $a_m(440)$, that incorporated reasonable value(s) of n', were generally consistent (e.g., appropriate order of magnitude) with the measurements of $a_{NAP}(440)$ (Fig. 5d). Secondly, the best fit linear least squares regression relationship ($r^2 = 0.40$) approached significance ($p = 0.1$), and was generally consistent with indications from the empirical PAV_m-based model (Fig. 5a). Third, the indicated positive y-intercept is consistent with a modest a_d component that, while poorly quantified, is generally acknowledged to be present, even in case 1 waters (Iturriaga and Siegel, 1989; Babin et al., 2003b; Wozniak and Stramski, 2004).

Summary and implications

This study has provided the most complete characterization of a and a_x in Lake Superior, confirming that it is an optically complex case 2 system. The findings have extended the limited literature for a_x and relationships with optically active constituents for lacustrine systems and particularly for the Laurentian Great Lakes. Differences among systems support the continued need for system-specific characterizations as presented here. The spectral features of a_{NAP} (S_{NAP}) and a_ϕ ($a_\phi(440) \div a_\phi(676)$) were similar to those reported for coastal marine and lacustrine case 2 systems. However, the S_{CDOM} values for Keewenaw Bay and open waters of Lake Superior were low relative to observations reported for other case 2 waters (and similar to S_{NAP}), suggesting an atypical composition for the lake's CDOM. a_{CDOM} was the dominant absorbing component through the blue and green wavelengths, representing ≥75% of $a(440)$ at all monitored locations in 2006. Spatial patterns of a_{CDOM} and a_{NAP} indicated the effects of terrigenous sources. A general gradient in a_{CDOM} and a_{NAP} extended from the Sturgeon River, through the bay, and into eastern Lake Superior in the 2006 survey. In contrast, a_ϕ was similar in Lake Superior and the bay during the survey of 2006. Differences in Fe content (e.g., FeXRI ÷ PAV_m) probably contributed to variations in the relationship between a_{NAP} and suspended solids, as represented by $a^*_{NAP,TSS}(440)$ and $a^*_{NAP,FSS}(440)$, reported here and elsewhere.

The absorption characteristics of Lake Superior (Figs. 2–4) present difficult challenges for effective remote sensing of Chl patterns, that are shared by many other lacustrine oligotrophic case 2 waters. The blue absorption peak is obscured by the other absorbing components, particularly CDOM (e.g., Fig. 4c and d). The red ($\lambda = 676$) peak alternative to estimate Chl may be compromised because this signal is overwhelmed by a_w (e.g., Fig. 4c and d). These conditions have doubtless contributed to the reported problems in remote sensing of Chl in the lake (Budd and Warrington, 2004; Li et al., 2004). The similarity of S_{CDOM} and S_{NAP} make it difficult to resolve the contributions of these two components through remote sensing.

The characterizations of a_x, and the relationships with optically active constituents, presented here, together with the recently reported backscattering information (Peng et al., 2009), will serve to support more robust remote sensing algorithm development and advance mechanistic approaches for Lake Superior. These characterizations meet specific recommendations made to support remote sensing initiatives for the lake (Gons and Auer, 2004; Gons et al., 2008). Moreover, this information can support parameterization of a mechanistic optics model for the underwater light field to simulate AOPs such as Secchi depth and the diffuse attenuation coefficient for downwelling irradiance (e.g., Effler et al., 2008).

This study has advanced the understanding of the role of minerogenic particles in contributing to a_{NAP}, based on analysis of paired SAX results. A widely held notion has been that a_{NAP} is dominated by a_d in case 1 waters as well as in many case 2 systems (Morel and Ahn, 1991; Babin et al., 2003b). The strong relationships between a_{NAP} and PAV_m (Fig. 5a), and a_{NAP} and FeXRI (Fig. 5b), reported here, provide compelling empirical evidence for the central role of terrigenous minerogenic particles in regulating the observed differences in a_{NAP} amongst these sites. In particular, this FeXRI relationship represents its first demonstration based on analysis of water column samples. Heretofore, such a relationship had only been anticipated, based on analysis of land-based sediment samples (Babin and Stramski, 2004). A central role of minerogenic particles was further supported by the consistency of predicted a_m values with a_{NAP} observations, obtained from the first set of forward method Mie theory calculations based on SAX data and reasonable literature values for n'.

Acknowledgments

Funding for this research was provided in part by Naval Research Laboratory for the "Lidar and hyperspectral remote sensing of the littoral environment" project. Sampling and field optical measurements were assisted by Tony Prestigiacomo aboard the U.S. Environmental Protection Agency's *R/V* Lake Guardian (pelagic waters of Lake Superior) and Michigan Technological University's *R/V* Agassiz (Keweenaw Bay). Laboratory analyses of absorption and chlorophyll *a* concentrations were performed by Lingsen Zhang and Whitney Forbes, respectively. U.S. EPA graciously contributed ship time aboard the *R/V* Lake Guardian to Michigan Tech as part of a cruise combining graduate instruction and value-added research. This is contribution 275 of the Upstate Freshwater Institute.

References

Babin, M., Stramski, D., 2004. Variations in the mass-specific absorption coefficient of mineral particles suspended in water. Limnol. Oceanogr. 49, 756–767.

Babin, M., Morel, A., Fournier-Siere, V., Fell, F., Stramski, D., 2003a. Light scattering properties of marine particles in coastal and open ocean waters as related to the particle mass concentration. Limnol. Oceanogr. 48, 843–859.

Babin, M., Stramski, D., Ferrari, G.M., Claustre, H., Bricaud, A., Obolensky, G., Hoepffner, N., 2003b. Variations in the light absorption coefficients of phytoplankton, nonalgal particles, and dissolved organic matter in coastal water around Europe. J. Geophys. Res. 108 (C7), 3211.

Binding, C.E., Jerome, J.H., Bukata, R.P., Booty, W.G., 2008. Spectral absorption properties of dissolved and particulate matter in Lake Erie. Remote Sens. Environ. 112, 1702–1711.

Blough, N.V., Green, S.A., 1995. Spectroscopic characterization and remote sensing of nonliving organic matter. In: Zepp, R.G., Sonntag, C. (Eds.), The Role of Nonliving Organic Matter in the Earth's Carbon Cycle. Wiley, pp. 23–45.

Bohren, C.F., Huffman, D.R., 1983. Absorption and Scattering of Light by Small Particles. John Wiley & Sons, New York.

Bowers, D.G., Harker, G.E.L., Stephan, B., 1996. Absorption spectra of inorganic particles in the Irish Sea and their relevance to remote sensing of chlorophyll. Int. J. Remote Sens. 17, 2449–2460.

Bricaud, A., Babin, M., Morel, A., Claustre, H., 1995. Variability in the chlorophyll-specific absorption coefficients of natural phytoplankton: analysis and parameterization. J. Geophys. Res. 100 (C7), 13,321–13,332.

Budd, J.W., 2004. Large-scale transport phenomena in the Keweenaw region of Lake Superior: the Ontonagon plume and the Keweenaw eddy. J. Great Lakes Res. 30 (Supplement 1), 467–480.

Budd, J.W., Warrington, D.S., 2004. Satellite-based sediment and chlorophyll a estimates for Lake Superior. J. Great Lakes Res. 30 (Supplement 1), 459–466.

Bukata, R.P., Jerome, J.H., Kondratyev, K.Y., Pozdnyakov, D.V., 1991. Estimation of organic and inorganic matter in inland waters: optical cross sections of Lakes Ontario and Ladoga. J. Great Lakes Res. 17, 461–469.

Carder, K.L., Steward, R.G., Harvey, G.R., Ortner, P.B., 1989. Marine humic and fulvic acids: their effects on remote sensing of ocean chlorophyll. Limnol. Oceanogr. 34, 68–81.

Clesceri, L.S., Greenberg, A.E., Eaton, A.D., 1998. Standard Methods for the Examination of Water and Wastewater20th ed. American Public Health Association, American Water Works Association, Water Environment Federation, Washington, D.C.

Cleveland, J.S., Weidemann, A.D., 1993. Quantifying absorption by aquatic particles: a multiple scattering correction for glass-fibre filters. Limnol. Oceanogr. 38, 1321–1327.

Del Vecchio, R., Blough, N.V., 2004. On the origin of the optical properties of humic substances. Environ. Sci. Technol. 38, 3885–3891.

Effler, S.W., 1996. Limnological and engineering analysis of a polluted urban lake. Prelude to Environmental Management of Onondaga Lake, New York. Springer-Verlag, New York, NY.

Effler, S.W., Gelda, R.K., Perkins, M.G., Peng, F., Hairston, N.G., Kearns, C.M., 2008. Patterns and modeling of the long-term optics record of Onondaga Lake, New York. Fund. Appl. Limnol. 172/3, 217–237.

Ferrari, G.M., Tassan, S., 1999. A method using chemical oxidation to remove light absorption by phytoplankton pigments. J. Phycol. 35, 1090–1098.

Gallegos, C.L., Neale, P.J., 2002. Partitioning spectral absorption in case 2 waters: discrimination of dissolved and particulate components. Appl. Opt. 41, 4220–4233.

Gons, H.J., Auer, M.T., 2004. Some notes on water color in Keweenaw Bay (Lake Superior). J. Great Lakes Res. 30 (Supplement 1), 481–489.

Gons, H.J., Auer, M.T., Effler, S.W., 2008. MERIS satellite chlorophyll mapping of oligotrophic and eutrophic waters in the Laurentian Great Lakes. Remote Sens. Environ. 112, 4098–4106.

Great Lakes National Program Office (GLNPO), 2009. Sampling and analytical procedures for GLNPO's open lake water quality survey of the Great Lakes. EPA 905-R-05-001. U.S. Environmental Protection Agency, Chicago, IL.

Helms, J.R., Stubbins, A., Ritchie Jason, D., Minor, E.C., Kieber, D.J., Mopper, K., 2008. Absorption spectral slopes and slope ratios as indicators of molecular weight, source, and photobleaching of chromophoric dissolved organic matter. Limnol. Oceanogr. 53, 955–969.

Iturriaga, R., Siegel, D.A., 1989. Microphotometric characterization of phytoplankton and detrital absorption properties in the Sargasso Sea. Limnol. Oceanogr. 34, 1706–1726.

Kirk, J.T.O., 1994. Light and Photosynthesis in Aquatic Ecosystems. Cambridge University, London.

Li, H., Budd, J.W., Green, S., 2004. Evaluation and regional optimization of bio-optical algorithms for central Lake Superior. J. Great Lakes Res. 30, 443–458.

Lohrenz, S.E., 2000. A novel theoretical approach to correct for pathlength amplification and variable sample loading in measurements of particulate spectral absorption by the quantitative filter technique. J. Plankton Res. 22, 639–657.

Loiselle, S.A., Bracchini, L., Dattilo, A.M., Ricci, M., Tognazzi, A., Cózar, A., Rossi, C., 2009. Optical characterization of dissolved organic matter using wavelength distribution of absorption spectral slopes. Limnol. Oceanogr. 54, 590–597.

Ma, X., Green, S.A., 2004. Photochemical transformation of dissolved organic carbon in Lake Superior – an in-situ experiment. J. Great Lakes Res. 30 (Supplement 1), 97–112.

Mitchell, B.G., Kahru, M., Wieland, J., Stramska, M., 2003. Determination of spectral absorption coefficients of particles, dissolved material and phytoplankton for discrete water samples (Chapter 4, Vol 4). Ocean Optics Protocols for Satellite Ocean Color Sensor Validation, Revision 4 Volumes 1–4. NASA/TM-2003-21621/Rev-Vol 1–4. National Aeronautical and Space Administration, Goddard Space Flight Center, MD.

Morel, A., Ahn, Y.-H., 1991. Optics of heterotrophic nanoflagellates and ciliates: a tentative assessment of their scattering role in oceanic waters compared to those of bacterial and algal cells. J. Mar. Res. 49, 177–202.

Morel, A., Prieur, L., 1977. Analysis of variations in ocean colour. Limnol. Oceanogr. 22, 709–722.

Morris, D.P., Hargreaves, B.T., 1997. The role of photochemical degradation of dissolved organic carbon in regulating the UV transparency of three lakes on the Pocono Plateau. Limnol. Oceanogr. 42, 239–249.

Owen, R.W., 1974. Optically effective area of particle ensembles in the sea. Limnol. Oceanogr. 19, 584–590.

Parsons, T.R., Maita, Y., Lalli, C.M., 1984. A Manual of Chemical and Biological Methods for Seawater Analysis. Pergamon Press, New York, NY.

Patterson, E.M., Gillette, D.A., Stockton, B.H., 1977. Complex index of refraction between 300 and 700 nm for Saharan aerosols. J. Geophys. Res. 82, 3153–3160.

Peng, F., Effler, S.W., 2005. Inorganic tripton in the Finger Lakes of New York: importance to optical characteristics. Hydrobiol. 543, 259–277.

Peng, F., Effler, S.W., 2007. Suspended minerogenic particles in a reservoir: light scattering features from individual particle analysis. Limnol. Oceanogr. 52, 204–216.

Peng, F., Effler, S.W., O'Donnell, D.M., Perkins, M.G., Weidemann, A.D., 2007. Role of minerogenic particles in light scattering in lakes and a river in Central New York. Appl. Opt. 46, 6577–6594.

Peng, F., Effler, S.W., O'Donnell, D.M., Weidemann, A.D., Auer, M.T., 2009. Characterization of minerogenic particles in support of modeling light scattering in Lake Superior through a two-component approach. Limnol. Oceanogr. 54, 1369–1381.

Perkins, M.G., Effler, S.W., Strait, C., Zhang, L., 2009. Light absorbing components in the Finger Lakes of New York. Fund. Appl. Limnol. 173/4, 305–320.

Perkins, M.G., Effler, S.W., Strait, C., 2010. Light absorption components in Onondaga Lake, New York. Fund. Appl. Limnol. 176/3, 209–223.

Pope, R.M., Fry, E.S., 1997. Absorption spectrum (380–700 nm) of pure water. II. Integrating cavity measurements. Appl. Opt. 36, 8710–8723.

Schwarz, J.N., Kowalczuk, P., Kaczmarek, S., Cota, F., Mitchell, B.G., Kahru, M., Chavez, F. P., Cunningham, A., McKee, D., Gege, P., Kishino, M., Phinney, D.A., Raine, R., 2002. Two models for absorption by coloured dissolved organic matter (CDOM). Oceanologia 44, 209–241.

Twardowski, M.S., Boss, E., Sullivan, J.M., Donaghay, P.L., 2004. Modeling the spectral shape of absorption by chromophoric dissolved organic matter. Mar. Chem. 89, 69–88.

Vodacek, A., Blough, N.V., DeGrandpre, M.D., Peltzer, E.T., Nelson, R.K., 1997. Seasonal variation of CDOM and DOC in the Middle Atlantic Bright: terrestrial inputs and photooxidation. Limnol. Oceanogr. 42, 674–686.

Wozniak, S.B., Stramski, D., 2004. Modeling the optical properties of mineral particles suspended in seawater and their influence on ocean reflectance and chlorophyll estimation from remote sensing algorithms. Appl. Opt. 43, 3489–3503.